Journal of
Materials Chemistry B

Accepted Manuscript

This is an *Accepted Manuscript*, which has been through the RSC Publishing peer review process and has been accepted for publication.

Accepted Manuscripts are published online shortly after acceptance, which is prior to technical editing, formatting and proof reading. This free service from RSC Publishing allows authors to make their results available to the community, in citable form, before publication of the edited article. This *Accepted Manuscript* will be replaced by the edited and formatted *Advance Article* as soon as this is available.

To cite this manuscript please use its permanent Digital Object Identifier (DOI®), which is identical for all formats of publication.

More information about *Accepted Manuscripts* can be found in the **Information for Authors**.

Please note that technical editing may introduce minor changes to the text and/or graphics contained in the manuscript submitted by the author(s) which may alter content, and that the standard **Terms & Conditions** and the **ethical guidelines** that apply to the journal are still applicable. In no event shall the RSC be held responsible for any errors or omissions in these *Accepted Manuscript* manuscripts or any consequences arising from the use of any information contained in them.

Journal of
Materials Chemistry B

RSC Publishing

ARTICLE

Effects of Surface Functionality of Carbon Nanomaterials on Short-Term Cytotoxicity and Embryonic Development in Zebrafish

Cite this: DOI: 10.1039/xoxxoooooox

Received ooth January 2012,
Accepted ooth January 2012

DOI: 10.1039/xoxxoooooox

www.rsc.org/

Raviraj Vankayala[1], Poliraju Kalluru[1], Hsin-Hui Tsai[1], Chi-Shiun Chiang[2], and Kuo Chu Hwang[1]*

Nanomaterials have been widely used in biomedical field as gene/drug carriers, magnetic resonance imaging ((MRI) contrast reagents, photothermal therapy reagents, fluorescent cellular markers, etc. The origins and working mechanisms of cytotoxicities of nanomaterials, however, are not well understood. It is often stated in the literature that a nanomaterial is non-toxic and biocompatible. In this study, we show that the short term cytotoxicity of a nanomaterial is determined by the surface functionality, rather than the core nanomaterial. A so-called "non-toxic and biocompatible" nanomaterial, such as, core/shell iron-filled carbon nanoparticles (Fe@CNPs) and nanodiamonds (NDs) can become cytotoxic when a cationic surface functionality, such as, imidazolium (IM) and tertiary methyl ammonium ethyl methacrylate (TMAEA) moieties, was grafted on the surface. To investigate the contributions of surface functionalities and the core nanomaterials on cytotoxicity, two "non-toxic and biocompatible" Fe@CNPs and NDs were surface-modified with different surface functionalities, including anionic COOH, zwitterionic PVP, neutral OH, cationic IM and TMAEA, and investigated for their cytotoxicities in both *in vitro* cancer cells (HeLa and U-87MG cells) and *in vivo* embryo developments of zebrafish. Among these surface functionalities, cationic IM and TMAEA functionalities of both Fe@CNPs) and NDs cause acute cytotoxicity to a similar extent in the *in vitro* cancer cell experiments, as well as affect severely the embryonic development and survival rates of zebrafish. Other surface functionalities do not show particularly strong cytotoxicities. To obtain information regarding the origins of cytotoxicities, the effects of surface functionalities were also examined on the lactate dehydrogenase (LDH) levels, cellular ROS generation, apoptosis, and changes in lysosomal membrane integrity, mitochondrial membrane potential, the intracellular pH (pH_i), and cell cycles. Our results clearly point out that surface functionality, rather than the core nanomaterials, play a critical role in dictating the short-term cytotoxicities.

Introduction

The innovation of nanotechnology has offered several new tools for the researchers working in the fields of biology and medicine[1]. In the recent years, nanomaterials were extensively used in biomedical applications, such as, imaging, gene delivery and drug delivery, etc[2-6]. The primary concerns for nanomaterials in biomedical applications are its biocompatibility and cost-effectiveness. Among various widely investigated nanomaterials, gold nanoparticles[7], silica nanoparticles[8], carbon nanoparticles[9], single and multi-walled carbon nanotubes[10,11], nanodiamonds (NDs)[12-14] and graphene[15-17] were often claimed to be biocompatible and non-toxic. Despite of this huge advancement in the field of nanobiomedicine, it is still unclear what key factors are responsible for the short term and long term cytotoxicities. To this end, several researchers have investigated the effects of size, shape and surface charge of nanomaterials on the nanoparticle-cell interactions and thereby the cytotoxicities in the biological system[18-21]. Recently, Rotello et al., has shown that in addition to the size, shape and surface charge, the carbon chain length of alkane thiol on the surface of the nanoparticle also play a major role in dictating cytotoxicity[12-24]. It was also reported that gold nanorods (Au NRs) with cetyl tetra ethyl ammonium bromide (CTAB) and poly (ethylene glycol) (PEG) also show huge differences in dictating the cytotoxicity as well as showing up/down-regulation of certain genes.[25] CTAB and PEG are detachable dispersants for nanomaterials. In another study, nano combinatorial library of carbon nanotubes with

diversified functionalities were developed and their cytotoxicities investigated[26]. It was shown that cytotoxicities occur via reduced protein binding, and altered immune responses in different cell lines[26]. However, no conclusive trend was found between surface functionalities of nanomaterials and short term cellular cytotoxicities.[9,26] Up to date, there are very limited number of papers reporting the correlation between surface functionalities of nanomaterials and the short term cytotoxicities.[9,26] In the literature, it is very often to see the term "X (X= silica nanoparticles, gold nanoparticles, nanodiamonds, etc) are non-toxic and biocompatible" without specifying the surface functionalities of these "non-toxic biocompatible" nanomaterials. Most of these researchers refer the cytotoxicity of nanomaterials to be originated from the core materials, rather than their surface functionalities. It is questionable whether the true origin for the cytotoxicity is coming from the core nanomaterial or from the surface functionality attached/grafted on the surface of nanomaterials.

To investigate whether the surface functionalities or the core nanomaterials are responsible for the short term cytotoxicities, we modify the core/shell iron-filled carbon nanoparticles (Fe@CNPs) and nanodiamonds (NDs) with different surface functionalities. Fe@CNPs is composed of metallic iron nanoparticles core and graphene layers shells, which have many olefinic C=C bonds for chemical modifications[27]. On the other hand, NDs are already well-known in the literature to act as a promising candidate for several biomedical applications[28,29]. In this study, we show that the short term/acute cytotoxicity of a nanomaterial is mainly determined by the surface functionality, rather than the core materials. We demonstrate that it is not scientifically correct to mention a nanomaterial to be "non-toxic and biocompatible" without specifying the surface functionality. Our work clearly indicates that selection of surface functional groups is more important than the core nanomaterials when choosing a nanomaterial for biomedical applications.

Materials and Methods

Synthesis of core/shell iron/carbon nanoparticles (Fe@CNPs) using solid state microwave arcing[27]: The magnetic core/shell iron encapsulated carbon nanoparticles were prepared by following the literature procedure. In brief, a $C_{60/70}$ and ferrocene (1:1 wt ratio) powder mixture together with small pieces of silicon (1x1x1~2x2x1 mm^3 from a broken silicon wafer) was irradiated with microwave inside a focused microwave oven (2.45 GHz, Discover system, CEM Corporation, USA) under an argon atmosphere (1 atm) for 15 s. The microwave irradiation process was repeated twice to have more completely carbonization of the carbon-containing powder. Finally, the magnetic products were collected using an external magnets, and structure characterization was performed in using a transmission electron microscope (TEM, Jeol, JEM-2100F, 200 kV).

Surface Graphitization of NDs[30]: Commercial NDs (Micron+, 0-0.25 μm, Element Six) were washed with dilute HCl and distillated water a few times and dried in a vacuum oven at 70 ^oC before thermal oxidation of surface residual functionalities in air at 480 ^oC for 6 h. Air-oxidized NDs were then put in a vacuum-sealed quartz tube, which was then thermally annealed in a furnace at 1200 ^oC for 1-3 h.

Surface functionalization of Fe@CNPs/NDs[30]: In a typical experiment, Fe@CNPs/NDs (50 mg) were suspended in 8 ml aqueous solution containing different monomers, such as, acrylic acid, N-vinyl pyrrolidone, 2-hydroxy ethyl methacrylate, and trimethyl ammonium ethyl methacrylate. The solution was then ultrasonicated in a bath-type ultrasonicator for 2 min to disperse the core/shell iron/carbon nanoparticles. A tetrahydrofuran (THF) solution (0.25 mL) containing benzoyl peroxide (22.5 mg) was added to the solution, followed by microwave irradiation for 10 s and ultrasonication for an additional 5 min. This process was repeated for 4 or 5 times with a total amount of 90–120 mg benzoyl peroxide (BPO) being added. The final solution was then diluted with deionized water, filtered through a nylon 66 (0.45 μm) membrane, and washed with deionized water several times to thoroughly remove free, unbound polymers from carbon nanomaterials. The above functionalized Fe@CNPs or NDs were well dispersed in aqueous solutions. For the surface functionalization of imidazolium cation, Fe@CNPs or NDs functionalized with 2-hydroxy ethyl methacrylate was chosen as a precursor and stirred for overnight in the presence of carbon tetra bromide (CBr_4) and dichloromethane (DCM) to replace the hydroxyl group with the bromine and subsequently, 1-methyl imidazole was added in acetonitrile solvent and vigorously refluxed for 40 h to obtain imidazolium cation functionalized Fe@CNPs or NDs. In order to introduce the fluorescence properties, an additional component, namely, Disperse Red 1 (DR1, 10 mg in 1 mL THF), was added, and the solution was sonicated and irradiated with microwave under the same conditions. The reason for adding the fluorescence moiety at the last stage of surface grafting is to avoid close contact with the graphene shells as the photoexcited fluorescence molecules can be quenched by the graphene shells on the Fe@CNPs and NDs surfaces.

Cell culture, materials and reagents: HeLa and U-87MG cells were grown in Dulbecco's Modified Eagle Medium (DMEM, Gibco, and Grand Island, NY, USA) supplemented with 10% heat-inactivated fetal bovine serum (Invitrogen, Carlsbad, CA, USA), 2 mM L-glutamine, 100 μg/mL penicillin and 100 U/mL of streptomycin. The cells were grown in a humidified incubator at 37°C (95% humidity, 5% CO2). Other chemicals were purchased from Sigma Aldrich (St. Louis, MO, USA).

Cytotoxicity assay: One milliliter of HeLa and U-87MG cells-containing solution (2.0×10^4 cells / mL) were added to each well of a 24-well plate and incubated for 1 day to allow the cells to stick on the surface of the plate. Aliquots of a PBS buffer solution containing different amounts of surface

functionalized Fe@CNPs and NDs were added to the 24-well plate, and the cell solutions were incubated for another 3 days. A 50 μL amount of a MTT aqueous solution (0.5 mg/mL) was added to each well of the 24-well plate 4 h before termination of the 3-days incubation, and the cells were allowed to incubate for another 4 h. Then, the upper layer of the solutions in the 24-well plate was discarded, and 1 mL of DMSO was added to each well to dissolve the violet color formazon product by pipette stirring. The final solution in each well was centrifuged at 13000 rpm to remove any solid residues before measurements of the optical absorbance at 570 nm. The optical absorbances were converted to cell viabilities based on a standard curve (absorbance vs cell numbers) obtained from controlled experiments carried out under the same condition except that no nanoparticles were added during cell culture processes.

Lactate dehydrogenase release (LDH) assay: 2×10^4 cells /mL of HeLa cells were loaded in a 24-well plate and incubated for 24 h. Fe@CNPs and NDs were added and further allowed it to interact for another 24 h. The cells were washed with PBS, trypsinized and centrifuged at 13000 rpm. 100 μL of the supernatant was transferred into another 96-well plate. To this, 100 μL of LDH reaction solution (Clontech Cytotoxicity Detection Kit, USA) was added and incubated for 30 min in the dark at room temperature. Before colorimetric detection at 490 nm, 1 M HCl was added to stop the enzymatic reaction.

Annexin-V apoptosis assay: HeLa cells were seeded into 6-well plates with the density of 2 x 10^5 cells per well. After 24 h, different surface functionalized Fe@CNPs/NDs stock solutions were added to the cells and incubated for 24 h. Cells were then trypsinized, aspirated and re-suspended in 500 μL binding buffer. Cells were further stained with FITC-Annexin-V (5 μL) and 7-AAD (5 μL) from the Annexin-V apoptosis detection kit (BD Biosciences, USA) and then keep it stand by for 15 min at room temperature in darkness, centrifuge at 1500 rpm for 5 min and then re-suspend in 1mL PBS, followed by flow cytometry analysis.

Reactive oxygen species (ROS) generation: HeLa cells were seeded into 6-well plates with the density of 2 x 10^5 cells per well. After 24 h, different surface functionalized Fe@CNPs/NDs stock solutions were added to the cells and incubated for 4 h. Cell culture medium was replaced with 2', 7'- dichlorofluorescein diacetate (DCFH-DA) solution (5 μM in cell culture medium) and incubated with cells for 30 min at 37 ^oC. Cells were then trypsinized and aspirated, followed by flow cytometry analysis. Green fluorescence was monitored.

Assessing the integrity of lysosomal membrane: The integrity of the lysosomal membrane was assessed quantitatively by flow cytometry. HeLa cells were seeded onto 6-well plates for 24 h and rinsed twice with PBS. Then different amounts of surface functionalized Fe@CNPs and NDs were added and incubated for another 24 h. After 24 h, the cells were washed twice with PBS and then incubated in serum medium with 5 μg/mL AO and 10% FBS for 15 min. Finally, the cells were washed to remove the free dye and then re-suspended in 1 mL PBS. AO positive cells were collected by flow cytometry using an excitation wavelength of 488 nm and an emission wavelength of 670 nm.

Mitochondrial membrane potential assay: HeLa cells were seeded onto 6-well plates for 24 h and rinsed twice with PBS. Then different amounts of surface functionalized Fe@CNPs/NDs were added and incubated for another 24 h. After 24 h, the cells were washed twice with 1X Assay buffer and then incubated in serum medium with 1 μg/mL mitochondrial JC-1 dye (Molecular Probes, USA) and 10% FBS for 15 min. Finally, the cells were washed to remove the free dye and then re-suspended in 1 mL of 1X Assay buffer. The ratio of fluorescence from FITC and PE channels were collected by flow cytometry using an excitation wavelength of 488 nm.

Analysis of Intracellular pH: HeLa cells were seeded onto 6-well plates for 24 h and rinsed twice with PBS. Then different amounts of surface functionalized Fe@CNPs and NDs were added and incubated for another 24 h. After 24 h, the cells were washed twice with PBS and then incubated in serum medium with 1 μg/ml BCECF-AM (2',7'-bis-(2-carboxyethyl)-5-(and-6)-carboxy fluorescein) (Molecular Probes, USA) and 10% FBS for 15 min. Finally, the cells were washed to remove the free dye and then re-suspended in 1 mL PBS. The ratio of fluorescence from FITC and PE channels were collected by flow cytometry using an excitation wavelength of 488 nm.

Cell cycle analysis: HeLa cells were seeded onto 6-well plates for 24 h and rinsed twice with PBS. Then different amounts of surface functionalized Fe@CNPs and NDs were added and incubated for another 24 h. After 24 h, the cells were washed twice with PBS and then trypsinized and fixed using 75% absolute ethanol under ice for 30 min. Further, Propidium iodide (PI) reagent (50 μg / ml) was used to stain the DNA and incubated at room temperature for 15 min. The cells were further washed with PBS to remove the unbound PI and then centrifuged for 5 min at 1500 rpm. The supernatant was discarded and the cell pellet was further re-suspended in 1 mL PBS.

Microinjection of different surface functionalized Fe@CNPs and NDs into Zebrafish Embryos: Wild-type AB strains of *Danio rerio* (zebrafish) embryos obtained from zebrafish core facility center, National Tsing Hua University were used in all the experiments. Fresh embryos were collected to the microinjection embryo tray just before the experiment. Different surface functionalized Fe@CNPs and NDs were diluted at appropriate concentrations in double distilled water and sonicated up until microinjection. Approximately 10 nL volume was microinjected into the animal pole region of embryos between stages 1 (one cell embryo) and 3 (four cell

embryo) using Drummond microinjector. Each experiment was performed on 50 embryos per condition. Following microinjection, embryos were transferred onto the petri dish filled with the system water and incubated at 28 oC in dark condition. For the in vivo cytotoxicity measurements, the live embryos were counted each day until 72 hpf (hours post fertilization). After the 72 hpf, all the developed embryos were hatched manually and examined the types of abnormalities undergone through fluorescence microscope (Nikon, E600).

Results and Discussion

Characterization of Fe@CNPs and NDs: The HR-TEM images clearly reveals that authentic Fe@CNPs (average size: 4~30 nm) has well-graphitized graphene shells (5~20 layers) with an iron nanoparticle core in the center, whereas NDs have an average particle size of 50-60 nm (see **Figure 1(A)**).

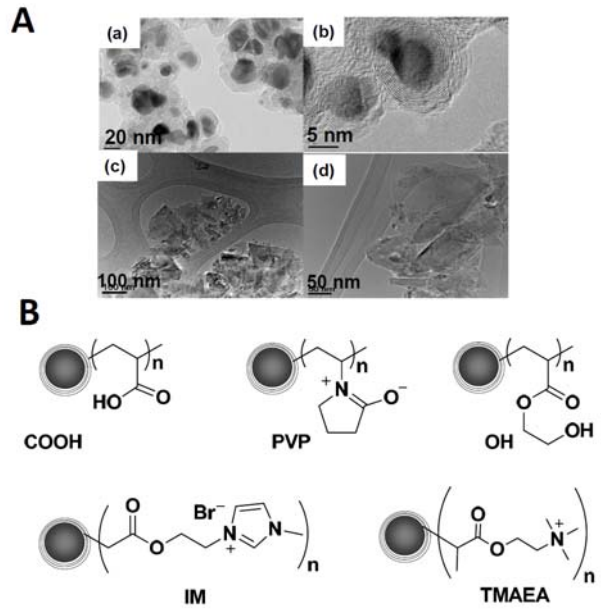

Figure 1. (A) HR-TEM images for surface functionalized Fe@CNPs/NDs. (B) Schematic representation for surface chemical structures of various Fe@CNPs/NDs.

The Fe@CNPs and NDs were subjected to surface modification by following a sonication-microwave irradiation process (see **Figure S1**)[9,30,31]. As the C=C double bonds on the surface graphene layers of Fe@CNPs and NDs are chemically reactive towards oligomeric radicals, many kinds of water soluble/fluorescent monomers can be grafted onto the surface. The chemical structures being grafted onto Fe@CNPs and NDs are listed in the Figure 1(B). These hydrophilic functional groups were chosen to introduce anionic (acid), cationic (imidazolium and tertiary methyl ammonium ethyl methacrylate), zwitter-ionic (vinyl pyrrolidone) and neutral (alcohol) charges onto Fe@CNPs (or NDs). After successful surface functionalization process, the Fe@CNPs/NDs can be separated from the free polymers and unreacted monomers in the solution by several cycles of ultra-centrifugation and solvent washing. The functional groups on the surface of Fe@CNPs and NDs were well characterized by FT-IR (see **Figure S2**). For carboxylic acid (poly (acrylic acids), PAA) moieties, the characteristic bands of acrylic acid appear at 3300~3600 cm^{-1} (strong and broad band for acidic O-H stretching), and 1728 cm^{-1} (acidic >C=O stretching). In the case of vinyl pyrrolidone (PVP), the characteristic bands appear at 3427 cm^{-1} (for broad ν_{O-H} stretching), 2927 cm^{-1} (weak band for alkyl ν_{C-H} stretching), and 1644 cm^{-1} (strong band for lactam >C=O stretching). The presence of the hydroxyl (OH) signal is due to the keto-enol form tautomerization of the pyrrolidone moiety. The characteristic broad band for the alkyl alcohol moiety appears at 2960 – 3200 cm^{-1}, in accompany with strong stretching signal at 1740 cm^{-1} (for ester >C=O stretching)[23,30]. For imidazolium (IM) and tertiary methyl ammonium ethyl methacrylate cation (TMAEA), the characteristic C=N, C=C and C=O stretchings were at 1570, 1627, and 1728 cm^{-1}, respectively. Since the surface functionalization of Fe@CNPs and NDs occurs on the outermost graphene layer, it does not cause any changes in their crystalline structures. In order to quantify the amount of surface functionality grafted on the nanoparticles, thermograviemetric analyses was performed for various functionalized Fe@CNPs or NDs (see **Figure S3**). As shown in Figure S3 (A) and (B), the onset of a rapid weight loss at ~500 ^oC is due to the degradation of the surface graphene layers for both Fe@CNPs as well as NDs. The oligomeric chains grafted to the surface of Fe@CNPs or NDs exhibit degradation at a temperature ranging 200~300 ^oC. Overall, the percentage weight loss of various functionalities of Fe@CNPs are, 12% for TMAEA, 11% for PVP, 15% for OH, 25% for IM and 16% for COOH, respectively, whereas for various surface functionalized NDs, the percentage weight loss is 20% for TMAEA, 11% for PVP, 18% for OH, 14% for IM and 11% for COOH, respectively. The average particle size distributions for the surface-functionalized Fe@CNPs and NDs were analyzed using dynamic light scattering (DLS) (see **Figure S4**) to be in the range of 80~100 nm, whereas for surface functionalized NDs the average particle size was 100~120 nm. The surface charges of water dispersible Fe@CNPs and NDs were determined via zeta-potential measurements (see **Figure S5)**. The Fe@CNPs and NDs with PAA, PVP and OH functional groups have net negative charges in the serum-free medium, whereas the IM and TMAEA groups exhibit net positive charges. However, all types of nanoparticles become negatively charged in the serum-containing medium, which is due to the adsorption of the negatively charged serum proteins onto the surface of these nanoparticles.

Cellular uptake and cytotoxicity assays. To induce cytotoxicity or to achieve efficient gene/drug delivery, it is essential for cells to have efficient cellular uptake of nanomaterials. Without examining the cellular uptake efficiencies, it is of no common grounds to compare the cytotoxicities of different nanomaterials. To this end, we have

first evaluated the cellular uptake efficiencies of various surface functionalized Fe@CNPs and NDs in HeLa cells by measuring the characteristic fluorescence emitted from Fe@CNPs and NDs using flow cytometry. The photoluminescence spectra in **Figure S6** clearly shows the broadband emission at 590 nm from the fluorescent oligomers, DR1 (Disperse Red 1, Sigma-Aldrich), on Fe@CNPs and NDs, respectively. The confocal images in **Figure 2(A)** show that most of the Fe@CNPs and NDs distribute homogenously throughout the cytoplasm region without entering into the nucleus. The cellular uptake percentages were also determined using flow cytometry after HeLa cells were fed with different surface functionalized Fe@CNPs and NDs.

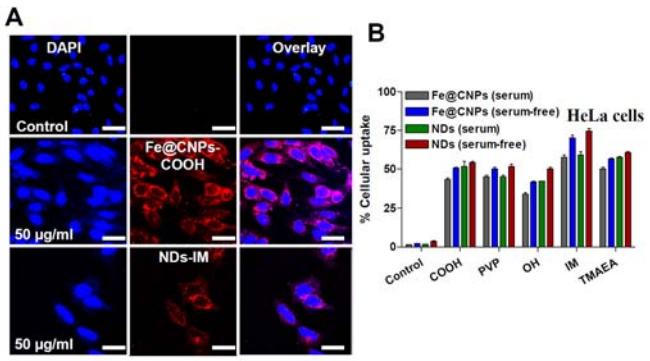

Figure 2. (A) Confocal laser scanning optical images of HeLa cells incubated with CNP-COOH and ND-IM for 4 h respectively. Control experiments are from HeLa cells without feeding nanoparticles. The cell nucleus is stained with DAPI dye (λ_{ex} = 405 nm and λ_{em} = 440 nm) and the red fluorescence is from the Rhodamine dye, which was monitored from the PI channel (λ_{ex} = 488 nm and λ_{em} = 570 nm). For all the images, the scale bar is 20 μm. (B) Cellular uptake of various surface functionalized Fe@CNPs/NDs monitored by flow cytometry in HeLa cells in serum and serum-free conditions. The concentrations of surface functionalized Fe@CNPs/NDs are 50 μg / mL.

In the literature many nanomaterials were assumed to have nearly 100% cellular uptake based on localized confocal fluorescence images[32], which might give a wrong conclusion of non-toxicity for a nanomaterial if a low cellular uptake is the case. The results in Figure 2(B) clearly reveal that all the surface functionalities grafted on Fe@CNPs and NDs exhibit ~65% cellular uptake efficiency in serum-free conditions. The uptake efficiencies were slightly hindered in the presence of serum, due to the non-specific binding of serum proteins on the surface of the cell membrane. To examine the cytotoxicity of different surface functionalized Fe@CNPs and NDs, MTT (3-(4,5-dimethylthiazolyl-2)-2,5-diphenyltetrazolium bromide) cell viability assay was performed. The cellular viabilities in **Figure 3(A)** and 3(B) clearly show that both Fe@CNPs and NDs induce dose-dependent cytotoxicity behaviours. As the core nanomaterials, Fe@CNPs/NDs are hydrophobic, it is not feasible to test its cytotoxicity due to its limitation in achieving water dispersibility. The half maximal inhibitory concentration (IC_{50}) values for OH, PVP, TMAEA and COOH-functionalized Fe@CNPs/NDs are more or less the same, ~100 μg/mL, whereas for cationic IM, the IC_{50} values are ~90 μg/mL for both Fe@CNPs-IM and NDs-IM in HeLa cells. To check whether or not the same cytotoxicity behaviour is observed in another tumor cell line, U-87MG cells were fed with different concentrations of various surface functionalized Fe@CNPs and NDs (see **Figure S7**). However, the IC_{50} values are similar to those of HeLa cells with very slight variations. The cytotoxicity behaviours of two different core nanomaterials (Fe@CNPs and NDs) are similar, when the same surface functionality was grafted on their surfaces. Among various surface functionalities, cationic IM and TMAEA induce significant cytotoxic effects than COOH, PVP, and OH. From the data above, one can see that the short term cytotoxicities of nanomaterials are mainly determined by the surface functionalities, but are weakly related to the core materials. From the data shown in Figure 3, it clearly shows that among various functionalities TMAEA is highly toxic in both Fe@CNPs/NDs. Furthermore, the surface functional group density of TMAEA was tuned by co-functionalization of trimethyl ammonium ethyl methacrylate (TMAEA) and 2-hydroxy ethyl methacrylate (OH) with different weight ratios. **Figure S8 (A)** shows the weight ratio of TMAEA vs. OH and the zeta-potential values of surface-functionalized Fe@CNPs
The FT-IR spectra shown in Figure S8 (B) confirms the successful functionalization process, in which the O-H stretching band at ~3430 cm^{-1} gradually decrease in company with gradual increase of the C-H stretching signal at ~2900 cm^{-1} from the methyl group of the TMAEA moiety from sample A to E, where the wt% of the TMAEA moiety increases from 0 to 100%. As the –C-N stretching signal corresponding to the tertiary methyl ammonium group does not exhibit any characteristic stretching band in the FT-IR. The peak area ratio for –O-H to the –C-H stretching bands was found to decrease dramatically upon increasing the wt% of TMAEA on surface layer (see Figure S8 (C)). Furthermore, MTT assay was also performed to monitor their respective HeLa cell viabilities after treating the samples A to E (see Figure S8(D)). The results in Figure S8 (D) exhibit a linear relationship between the short term cytotoxicity to the amount of the cationic TMAEA moiety, indicating that it is the TMAEA moiety which is causing the short term cytotoxicity.

To further investigate the origins of the cytotoxicities induced by various surface functionalities, we determine the Lactate dehydrogenase (LDH) levels. LDH is a characteristic assay to assess the cellular membrane integrity of the cells in the culture medium[33]. The results in **Figure 4** shows the LDH release profiles from HeLa cells after treatment with various surface functionalized Fe@CNPs/NDs. When HeLa cells exposed to different concentrations of surface functionalized Fe@CNPs and NDs, the LDH levels for cationic IM and TMAEA are higher than COOH, PVP and OH for both Fe@CNPs and NDs. Overall, our cellular uptake and cytotoxicity results suggest that the differences in the cytotoxicity behaviours are not due to the differences in the cellular uptake efficiencies, rather solely due to the functional groups attached on their surfaces.

ROS generation and Annexin V apoptosis assay: Induction of oxidative stress is a major toxicological paradigm for many

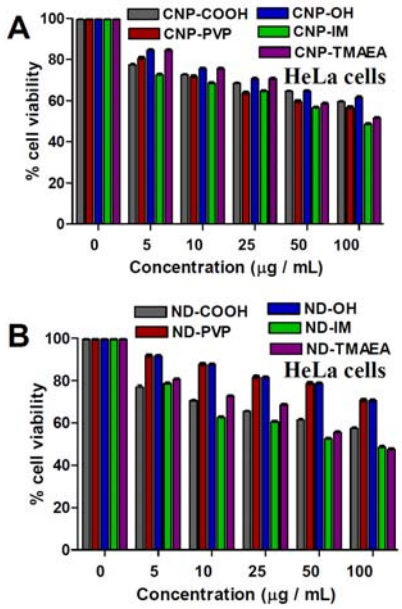

Figure 3. Cell viabilities by MTT assay in the presence of different concentrations of various surface functionalized (A) Fe@CNPs and (B) NDs in HeLa cells respectively.

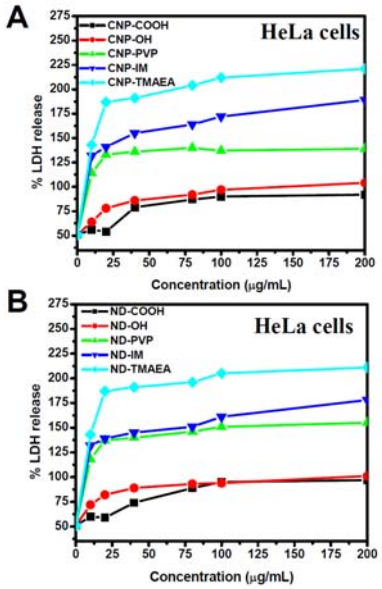

Figure 4. LDH assay for various surface functionalized (A) Fe@CNPs and (B) NDs at different concentrations in HeLa cells respectively.

nanomaterials[34]. To examine the induction of oxidative stress by different surface functionalized Fe@CNPs and NDs, we monitor the cellular ROS generation by flow cytometry using a reductive reagent, non-fluorescent 2',7'–dichlorofluorescein diacetate (DCFH-DA), which can be oxidized by intracellular ROS to become fluorescent 2',7'–dichlorofluorescein (DCF). HeLa cells were treated with various surface functionalized Fe@CNPs and NDs for 24 h under reduced serum conditions.

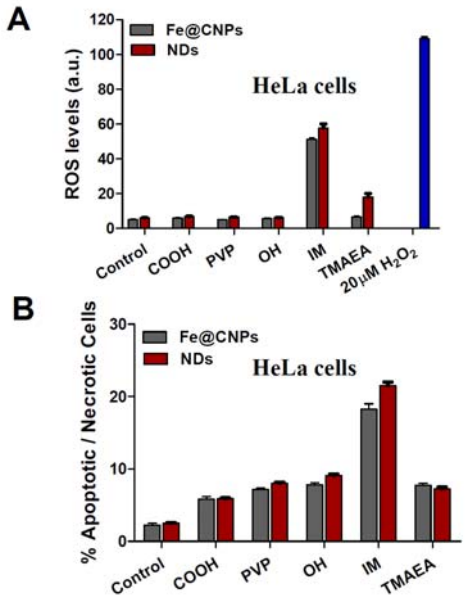

Figure 5. (A) ROS generation monitored using flow cytometry for various surface functionalized Fe@CNPs/NDs in HeLa cells. (B) Apoptosis detection by Annexin-V assay in HeLa cells treated with various surface functionalized Fe@CNPs/NDs. The concentrations of surface functionalized Fe@CNPs/NDs are 50 μg / mL.

Since the IC_{50} values for various surface functionalized Fe@CNPs and NDs is ~100 μg/mL, we chose an optimum concentration of 50 μg/mL for further experiments. From **Figure 5(A)**, it clearly indicates that the ROS levels induced by cationic IM are ~6 times higher than the control. In contrast, the other functional groups have ROS levels similar to that of untreated control. The increased levels of ROS for IM-modified Fe@CNPs and NDs are due to their cationic charges in nature, which can disrupt the negatively charged cell membrane and their cellular components via electrostatic interactions, leading to the elevated levels of ROS. ROS has been identified as an inducer of cell apoptosis[35]. Besides ROS, we further determine the percentage of apoptotic and necrotic cells using Annexin-V dye by flow cytometry. Cells were treated with different surface-functionalized Fe@CNPs and NDs under the same conditions as those in the ROS experiments. From Figure 5(B), it was clearly evident that cationic IM has generated ~25% of apoptotic and necrotic cells. As compared to the IM functionality, the cationic TMAEA is less cytotoxic, which is probably due to slightly higher steric hindrance from three methyl groups on ammonium cation center and thus less strong electrostatic interactions with proteins and poly anionic DNAs in the host cells. These results confirm that IM functional group exhibits higher cytotoxicity. Therefore, it can be concluded that surface functionality plays a very important role in inducing both oxidative stress and apoptosis. It is notable that the rest of functionalized Fe@CNPs and NDs did not induce significant levels of apoptosis, albeit, the ROS was induced to the similar extent. A thermodynamic and spectroscopic observation reveals that imidazolium-based ionic liquids can bind to the tryptophan

residues of bovine serum albumin proteins (BSA) tightly[36,37]. Therefore, it is also possible that the cationic IM moieties interact with proteins and poly-anionic DNAs inside the cells in a similar way.

Changes in lysosomal membrane integrity and mitochondrial membrane potential assay: Previously, several studies report that nanomaterials can enter into and accumulate in the endosome/lysosomal regions, leading to damages in the integrity of the lysosomal membrane and subsequent release of the nanomaterials into the other organelles[38-40].

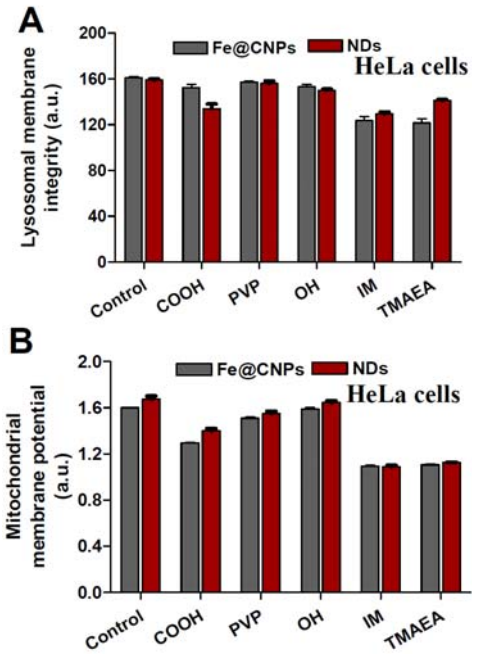

Figure 6. (A) Lysosomal membrane integrity monitored by flow cytometry using Acridine orange staining. Bar diagram representing the changes in the mean fluorescence intensities of Acridine orange monitored for various surface functionalized Fe@CNPs/NDs. (B) Changes in mitochondrial membrane potentials monitored using JC-1 dye for various surface functionalized Fe@CNPs/NDs in HeLa cells. The concentrations of surface functionalized Fe@CNPs/NDs are 50 µg / mL.

In the present study, Acridine Orange (AO) was used as a probe to study the integrity of the lysosomal membrane to examine which type of surface functionality can possibly cause the damage to the lysosomal membrane integrity. **Figure 6(A)** shows that the changes in the AO fluorescence intensities were similar to that of the control ones for all the surface functionalized Fe@CNPs/NDs. In sharp contrast, cationic IM modified Fe@CNPs and NDs have induced more pronounced changes in the membrane integrity as compared to the other surface functional groups. The results clearly show that nanomaterials grafted with cationic imidazolium moiety, disregarding what the core nanomaterial is Fe@CNPs or ND, could certainly target at mitochondria and induce acute cytotoxicity. It is well-known that the mitochondrion takes part in the oxidative phosphorylation and functions as the energy factory of cells[41]. The mitochondrion-specific dye JC-1 was used to detect changes in mitochondrial membrane potential by using flow cytometry. Apoptotic cells mainly show green fluorescence, while healthy cells show red and green fluorescence, making JC-1 suitable for the detection of mitochondrial damages[42]. From Figure 6(B) it clearly shows that cationic IM and TMAEA exhibit a significant drop in the ratio of the red to green fluorescence intensities of JC-1 dye, whereas other surface functionalities do not cause changes in the mitochondrial membrane potentials. The data in Figure 6(B) clearly indicate that cationic IM and TMAEA functionalities might disrupt the cellular metabolism, release reactive oxygen species from the mitochondria, and even cause apoptosis. Eventually, IM and TMAEA surface functionalities might localize in the mitochondria, and thereby disrupt the production of ATP energy molecules, and then cause increases in the cytoplasmic oxidative stress.

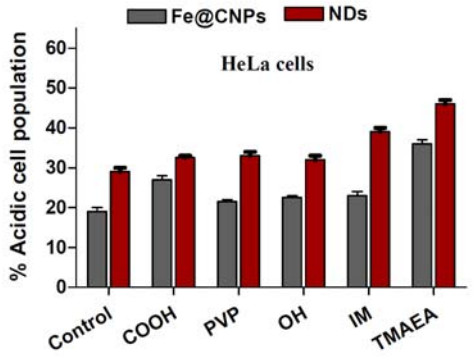

Figure 7. (A) Acidic cell population (intracellular pH, pH_i) monitored by flow cytometry for various surface functionalized Fe@CNPs/NDs in HeLa cells respectively. The concentrations of surface functionalized Fe@CNPs and NDs are 50 µg / mL.

Intracellular pH. The intracellular pH (pHi) appears to be closely involved in the regulation of many metabolic pathways, including glycolysis and gluconeogenesis, and its maintenance within a narrow range provides the appropriate environment for wide varieties of intracellular activities[45,46]. In most of cases, apoptosis has been induced either through signalling mechanisms or chemical stress which is associated with the intracellular acidification process. A fluorescent probe BCECF (2',7'-bis-(2-carboxyethyl)-5,6-carboxyfluorescein) was used to monitor the changes in the intracellular pH levels by using flow cytometry. **Figure 7** clearly shows that cationic TMAEA functionality induces ~60% of acidic cell populations, which might be the reason responsible for high level of apoptosis-mediated cell death. The acidic population levels for other surface functionalized Fe@CNPs/NDs are similar to that of the untreated cells.

Cell cycle analysis: Cell cycle is a series of events that lead to cell division and replication. The whole cell cycle mainly progresses in four different phases, such as, G1, S, G2 and M. The interaction of nanoparticles with cells usually depends on the cell cycle, because of the expression of membrane proteins [45]. It is also believed that the uptake of nanomaterials is

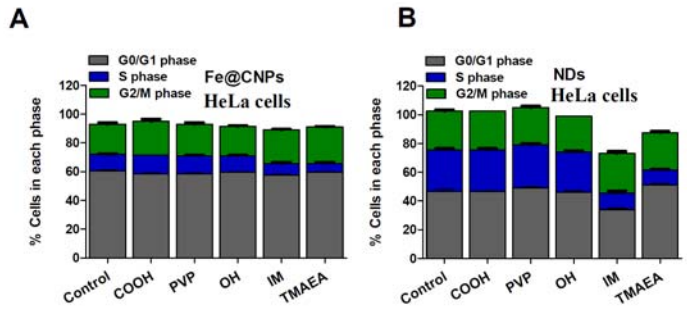

Figure 8. (A) Cell cycle analyses of HeLa treated with various surface functionalized (A) Fe@CNPs and (B) NDs for 24 h respectively. The bar graphs indicate the changes in the cell cycle progression. The concentrations of surface functionalized Fe@CNPs/NDs are 50 µg / mL.

strongly dependent on which particular phase the cells are being progressed[46]. However, the effect of surface functionality of carbon nanomaterials on the cell cycle progression was never reported before. **Figure 8(A)** and (B) show that when compared with that of untreated control, cationic IM and TMAEA functionalities exhibit distinct effects on the cell cycle distribution in HeLa cells under serum-free conditions. In sharp contrast, only cells that are progressing into S-phase are affected. This means that the cells treated with cationic IM and TMAEA-functionalized nanomaterials, disregarding whether the core material is Fe@CNPs or ND, can block the proliferation or the DNA synthesis phase of the cells. The most probable reason is that the net positive charges of IM and TMAEA interact strongly with poly-anionic DNA, and thereby hinder the cell proliferation rate. This phenomenon also holds true for the toxic cationic drugs bind to the DNA groove tightly to suppress the cell proliferation and induce cytotoxicity[47].

Biocompatibility of surface functionalized Fe@CNPs and NDs in zebrafish: To study the biocompatibility of surface functionalized Fe@CNPs and NDs on the embryonic development of zebrafish, nanoparticles were microinjected during 8-cell stage of the embryos. From **Figure S8,** different surface functionalities exhibit different survival rates of zebrafish. For both Fe@CNPs and NDs, cationic IM and TMAEA cause significant drops in their survival rates. Control experiments were also done by microinjecting DI water and a set of embryos without microinjection to compare the survival rate of zebrafish under the same experimental conditions. Cardiac malformation, yolk-sac and head edema were the most frequently observed abnormalities in zebrafish treated with Fe@CNPs and NDs functionalized with IM and TMAEA (see **Figure 9**).

The percentages of abnormalities induced by various functional groups for both Fe@CNPs and NDs were summarized in **Figure S9**. The abnormalities such as cardiac malformation, yolk-sac and head edema induced by the cationic IM and TMAEA functionalities is presumably due to the elevated levels of ROS and up/down regulation of certain genes, which are similar to that observed in the zebrafish treated with

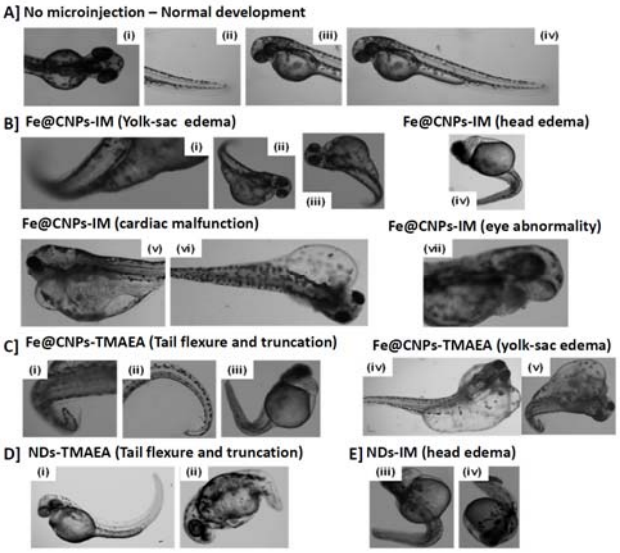

Figure 9. Abnormalities observed in zebrafish after microinjection of various surface functionalized Fe@CNPs and NDs at 120 hpf. (A) No microinjection and zebrafish developed under normal development. (B) Fe@CNPs-IM (i, ii, iii) represents yolk-sac edema, (iv) represents head edema, (v, vi) represents cardiac malfunction and (vii) eye abnormality. (C) Fe@CNPs-TMAEA (I, ii, iii) represents tail flexure and truncation, (iv, v) represents yolk-sac edema. (D) NDs-TMAEA (i, ii) represents tail flexure and truncation. (E) NDs-IM (iii, iv) represents head edema.

Ag NPs, iron oxide NPs, dichloroacetic acid and cadmium[48-50]. Moreover, the accumulated Fe@CNPs and NDs can also alter the diffusion and interactions of biomolecules (for example, nucleic acids, proteins, such as transcription factors and signaling molecules) leading to the interference or malfunctioning of various signalling cascades[48]. Overall, our results indicate that both the cationic IM and TMAEA surface functionalities of carbon nanomaterials are very cytotoxic by inducing several cellular events, LDH leakage of cellular membranes, elevated levels of ROS, increase in acidic cell and apoptotic populations, lowering mitochondrial membrane potentials, losing lysosomal membrane integrity, arresting the S-phase in cell cycle, and also in the embryonic development of zebrafish (see **Figure 10**).

Cationic IM and TMAEA functional groups are considered to be highly toxic, whereas other anionic COOH, neutral OH and zwitterionic PVP show low cytotoxicities. In the literature, various types of nanovectors were used to carry DNAs, siRNAs, fluorescent molecules and anticancer drugs for different biomedical applications[51]. In order to have efficient cellular internalization with the negatively charged cellular membranes and also to have effective complexation with the negatively charged small molecules, such as nucleic acids, nanocarriers bearing cationic surface charge are widely used (for example, cationic polymers and lipids)[31,32]. Our results clearly suggest that nanomaterials bearing cationic surface functionalities, such as IM and TMAEA, are not suitable as nanocarriers, since the nanovectors itself are capable of inducing severe short-term toxicity to the biological systems. Note that the cellular MTT data show no obvious difference between IM and TMAEA.

Table 1. Summary of the abnormalities in zebrafish induced after microinjection of various surface functionalized Fe@CNPs and NDs.

Summary for the Mutations in zebra fish after microinjection of various surface functionalized Fe@CNPs/NDs					
Fe@CNPs/NDs-F.G	Yolk Sac Edema	Head Edema	Cardiac Malfunction	Eye Abnormality	Tail Flexure and Truncation
CNP-COOH	+ (9%)	+ (6%)	-	-	+ (8%)
CNP-PVP	-	-	-	-	+ (4%)
CNP-OH	-	-	-	-	+(5%)
CNP-IM	+ (13%)	+ (8%)	+ (15%)	+ (4%)	-
CNP-TMAEA	+ (8%)	+ (6%)	-	-	+ (11%)
ND-COOH	+ (11%)	+ (4%)	-	+ (2%)	+ (12%)
ND-PVP	+ (2%)	-	-	-	+ (2%)
ND-OH	+(3%)	-	-	-	+(1%)
ND-IM	+ (15%)	+ (10%)	+ (18%)	+ (2%)	+ (1%)
ND-TMAEA	+ (4%)	+ (7%)	-	-	+ (8%)

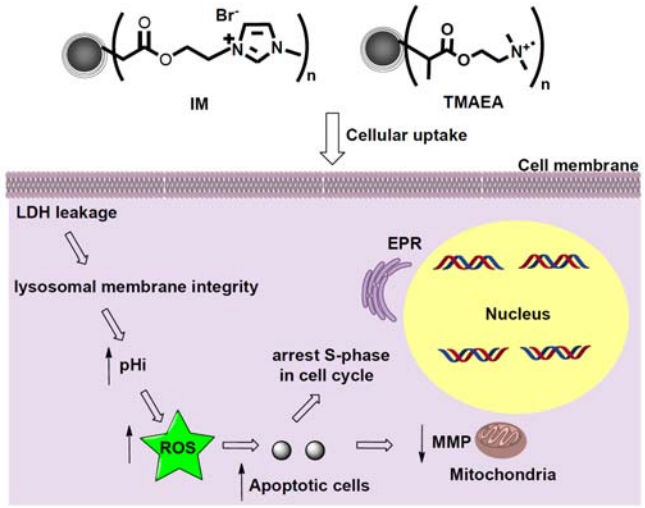

Figure 10. Schematic representation for the cellular events monitored for IM and TMAEA functionalized Fe@CNPs/NDs.

However the LDH release level of TMAEA treated cells was higher than that of IM treated cells. In terms of ROS level, IM was higher. The results indicate that elevated ROS and LDH release level may result in mutation of organs and/or abnormal cellular functions, but may not lead to cellular deaths as determined by the MTT assay.

Conclusions

We have investigated the *in vitro* and *in vivo* biocompatibilities of nanomaterials by changing the surface functionalities (including, anionic -COOH, zwitter-ionic PVP, neutral OH, cationic IM and TMAEA), as well as the core nanomaterials, i.e., the Fe@CNPs and NDs. Our results clearly show that the short-term cytotoxicity observed in most of the cancer cells as well as in the embryonic development of zebrafish mainly originates from the surface functional groups, and is independent of the core nanomaterials. Among the surface functionalities investigated, cationic IM and TMAEA surface functional groups are the most toxic to cells via disruption of the cell membrane, causing LDH leakage into the culture medium, targeting at mitochondria, lowering their membrane potentials, increasing in the intracellular pH levels, causing lysosomal membrane degradation, and finally inhibiting the cell proliferation by blocking the DNA synthesis (S-phase). In contrast, the other functional groups, such as, anionic -COOH, zwitterionic PVP and neutral OH, do not exhibit noticeable cytotoxic effects under identical experimental conditions and similar extents of cellular uptake efficiencies. In the case of *in vivo* zebrafish model system, cationic IM and TMAEA functionalities cause severe abnormalities in the development of zebrafish and also decrease in the survival rate. Other surface functional groups, such as, -COOH, PVP and OH, do not induce any abnormalities and survival rates in zebrafish. When attached with the toxic surface functional groups, such as, cationic IM and TMAEA, so-called "non-toxic and biocompatible" nanomaterials, such as, NDs, may also become very cytotoxic and non-biocompatible. Overall, our results clearly show that the key determining factor for short term cytotoxicity of nanomaterials is the surface functionality, rather than the core nanomaterials. It is therefore not scientifically correct to state that "X" (X= silica nanoparticles, gold nanoparticles, nanodiamonds, etc.) are non-toxic and biocompatible without specifying the surface functionalities on these nanomaterials. To surface-modified nanomaterials for biomedical applications, toxic cationic functional groups should be avoided.

Acknowledgements

The authors are grateful to the financial support from the Frontier Research Center on Fundamental and Applied Sciences of Matters, National Tsing Hua University and the National Science Council, Taiwan.

Notes and references

[1]Department of Chemistry, [2]Department of Biomedical Engineering and Environmental Sciences, National Tsing Hua University, Hsinchu 30013, Taiwan. **Email:* kchwang@mx.nthu.edu.tw

Electronic Supplementary Information (ESI) available: Schematic for surface functionalization process, FT-IR, DLS, zeta-potential, PL spectra, cell viability in U-87MG cells and zebrafish survival rates. See DOI: 10.1039/b000000x/

1. C. Harrison, *Nat Rev Drug Discov*, 2013, **12**, 264-264.
2. S. J. Shin, J. R. Beech and K. A. Kelly, *Integrative Biology*, 2013, **5**, 29-42.
3. S. Jin, J. Leach and K. Ye, in *Micro and Nano Technologies in Bioanalysis*, eds. R. S. Foote and J. W. Lee, Humana Press2009, vol. 544, ch. 34, pp. 547-557.

4. J. Zhang, Y. Lei, A. Dhaliwal, Q. K. T. Ng, J. Du, M. Yan, Y. Lu and T. Segura, *Biomacromolecules*, 2011, **12**, 1006-1014.
5. D. He, X. He, K. Wang, M. Chen, Y. Zhao and Z. Zou, *Journal of Materials Chemistry B*, 2013, **1**, 1552-1560.
6. N. Z. Knezevic and V. S. Y. Lin, *Nanoscale*, 2013, **5**, 1544-1551.
7. Ž. Krpetić, I. Singh, W. Su, L. Guerrini, K. Faulds, G. A. Burley and D. Graham, *Journal of the American Chemical Society*, 2012, **134**, 8356-8359.
8. S. A. Mackowiak, A. Schmidt, V. Weiss, C. Argyo, C. von Schirnding, T. Bein and C. Bräuchle, *Nano Letters*, 2013, **13**, 2576-2583.
9. Q. Mu, L. Yang, J. C. Davis, R. Vankayala, K. C. Hwang, J. Zhao and B. Yan, *Biomaterials*, 2010, **31**, 5083-5090.
10. S. Alidori, K. Asqiriba, P. Londero, M. Bergkvist, M. Leona, D. A. Scheinberg and M. R. McDevitt, *The Journal of Physical Chemistry C*, 2013, **117**, 5982-5992.
11. J. C. Carrero-Sánchez, A. L. Elías, R. Mancilla, G. Arrellín, H. Terrones, J. P. Laclette and M. Terrones, *Nano Letters*, 2006, **6**, 1609-1616.
12. X.-Q. Zhang, M. Chen, R. Lam, X. Xu, E. Osawa and D. Ho, *ACS Nano*, 2009, **3**, 2609-2616.
13. P. Zhang, J. Yang, W. Li, W. Wang, C. Liu, M. Griffith and W. Liu, *Journal of Materials Chemistry*, 2011, **21**, 7755-7764.
14. I. P. Chang, K. C. Hwang and C.-S. Chiang, *Journal of the American Chemical Society*, 2008, **130**, 15476-15481.
15. H. Kim, R. Namgung, K. Singha, I.-K. Oh and W. J. Kim, *Bioconjugate Chemistry*, 2011, **22**, 2558-2567.
16. H. Kim and W. J. Kim, *Small*, 2013, DOI: 10.1002/smll.201202636.
17. K. Wang, J. Ruan, H. Song, J. Zhang, Y. Wo, S. Guo and D. Cui, *Nanoscale Res Lett*, 2011, **6**, 8.
18. Y. Pan, S. Neuss, A. Leifert, M. Fischler, F. Wen, U. Simon, G. Schmid, W. Brandau and W. Jahnen-Dechent, *Small*, 2007, **3**, 1941-1949.
19. R. Coradeghini, S. Gioria, C. P. García, P. Nativo, F. Franchini, D. Gilliland, J. Ponti and F. Rossi, *Toxicology Letters*, 2013, **217**, 205-216.
20. A. M. El Badawy, R. G. Silva, B. Morris, K. G. Scheckel, M. T. Suidan and T. M. Tolaymat, *Environmental Science & Technology*, 2010, **45**, 283-287.
21. X. Zhao, S. Ng, B. Heng, J. Guo, L. Ma, T. Tan, K. Ng and S. Loo, *Arch Toxicol*, 2013, **87**, 1037-1052.
22. A. Chompoosor, K. Saha, P. S. Ghosh, D. J. Macarthy, O. R. Miranda, Z.-J. Zhu, K. F. Arcaro and V. M. Rotello, *Small*, 2010, **6**, 2246-2249.
23. K. Saha, S. T. Kim, B. Yan, O. R. Miranda, F. S. Alfonso, D. Shlosman and V. M. Rotello, *Small*, 2013, **9**, 300-305.
24. S. T. Kim, K. Saha, C. Kim and V. M. Rotello, *Accounts of Chemical Research*, 2013, **46**, 681-691.
25. C. Grabinski, N. Schaeublin, A. Wijaya, H. D'Couto, S. H. Baxamusa, K. Hamad-Schifferli and S. M. Hussain, *ACS Nano*, 2011, **5**, 2870-2879.
26. H. Zhou, Q. Mu, N. Gao, A. Liu, Y. Xing, S. Gao, Q. Zhang, G. Qu, Y. Chen, G. Liu, B. Zhang and B. Yan, *Nano Letters*, 2008, **8**, 859-865.
27. Y.-C. Liang, K. C. Hwang and S.-C. Lo, *Small*, 2008, **4**, 405-409.
28. Y. Zhu, J. Li, W. Li, Y. Zhang, X. Yang, N. Chen, Y. Sun, Y. Zhao, C. Fan and Q. Huang, *Theranostics*, 2012, **2**, 302-312.
29. X. Zhang, S. Wang, M. Liu, J. Hui, B. Yang, L. Tao and Y. Wei, *Toxicology Research*, 2013.
30. I. P. Chang, K. C. Hwang, J.-a. A. Ho, C.-C. Lin, R. J. R. Hwu and J.-C. Horng, *Langmuir*, 2009, **26**, 3685-3689.
31. Y.-L. Hsin, J.-Y. Lai, K. C. Hwang, S.-C. Lo, F.-R. Chen and J. J. Kai, *Carbon*, 2006, **44**, 3328-3335.
32. T. Wang, J. Bai, X. Jiang and G. U. Nienhaus, *ACS Nano*, 2012, **6**, 1251-1259.
33. X. Han, R. Gelein, N. Corson, P. Wade-Mercer, J. Jiang, P. Biswas, J. N. Finkelstein, A. Elder and G. Oberdörster, *Toxicology*, 2011, **287**, 99-104.
34. H. Yang, C. Liu, D. Yang, H. Zhang and Z. Xi, *Journal of Applied Toxicology*, 2009, **29**, 69-78.
35. F. T. Andón and B. Fadeel, *Accounts of Chemical Research*, 2012, **46**, 733-742.
36. F. Geng, L. Zheng, J. Liu, L. Yu and C. Tung, *Colloid Polym Sci*, 2009, **287**, 1253-1259.
37. Y. Shu, M. Liu, S. Chen, X. Chen and J. Wang, *The Journal of Physical Chemistry B*, 2011, **115**, 12306-12314.
38. J. S. Teodoro, A. M. Simões, F. V. Duarte, A. P. Rolo, R. C. Murdoch, S. M. Hussain and C. M. Palmeira, *Toxicology in Vitro*, 2011, **25**, 664-670.
39. S. Bhattacharjee, D. Ershov, K. Fytianos, J. van der Gucht, G. Alink, I. Rietjens, A. Marcelis and H. Zuilhof, *Part Fibre Toxicol*, 2012, **9**, 1-19.
40. E. Fröhlich, C. Meindl, E. Roblegg, B. Ebner, M. Absenger and T. Pieber, *Part Fibre Toxicol*, 2012, **9**, 1-13.
41. M. H. Allen, K. N. Day, S. T. Hemp and T. E. Long, *Macromolecular Chemistry and Physics*, 2013, **214**, 797-805.
42. M. Das and S. K. Sahoo, *PLoS ONE*, 2012, **7**, e32920.
43. C. S. Parkins, J. A. Chadwick and D. J. Chaplin, *Br J Cancer Suppl*, 1996, **27**, S75-77.
44. Y. Tian, A. Glogowska, W. Zhong, T. Klonisch and M. Xing, *Journal of Materials Chemistry B*, 2013.
45. L. A. Austin, B. Kang, C.-W. Yen and M. A. El-Sayed, *Bioconjugate Chemistry*, 2011, **22**, 2324-2331.
46. J. A. Kim, C. Aberg, A. Salvati and K. A. Dawson, *Nat Nano*, 2012, **7**, 62-68.
47. M. O. Fenley, R. C. Harris, B. Jayaram and A. H. Boschitsch, *Biophysical Journal*, 2010, **99**, 879-886.
48. K. J. Lee, P. D. Nallathamby, L. M. Browning, C. J. Osgood and X.-H. N. Xu, *ACS Nano*, 2007, **1**, 133-143.
49. F. E. Williams, T. J. Sickelbaugh and E. Hassoun, *Journal of Biochemical and Molecular Toxicology*, 2006, **20**, 183-190.
50. A. V. Hallare, M. Schirling, T. Luckenbach, H. R. Köhler and R. Triebskorn, *Journal of Thermal Biology*, 2005, **30**, 7-17.
51. C. Y. Cheung, N. Murthy, P. S. Stayton and A. S. Hoffman, *Bioconjugate Chemistry*, 2001, **12**, 906-910.

Table of Content Graphic

Cationic surface functionalities of nanomaterials, such as, imidazolium and trimethylammonium ethyl methacrylate induce strong cytotoxicity *in-vitro* and in zebrafish.